

## Current outflow to low-density plasma region of z-pinch with pre-embedded axial magnetic field

M. Cvejić<sup>1</sup>, D. Mikitchuk<sup>1</sup>, R. Doron<sup>1</sup>, E. Kroupp<sup>1</sup>, C. Stollberg<sup>1</sup>, A.L. Velikovich<sup>2</sup>,  
J.L. Giuliani<sup>2</sup>, E.P. Yu<sup>3</sup>, A. Fruchtmann<sup>4</sup>, Y. Maron<sup>1</sup>

<sup>1</sup> *Weizmann Institute of Science, Rehovot 7610001, Israel*

<sup>2</sup> *Plasma Physics Division, Naval Research Laboratory, Washington, D.C. 20375, USA*

<sup>3</sup> *Sandia National Laboratories, P.O. Box 5800, Albuquerque, NM 87185-1186, USA*

<sup>4</sup> *Holon Institute of Technology, P.O. Box 305, Holon 58102, Israel*

### 1. INTRODUCTION

Magnetic flux compression can be achieved within a conducting shell when the shell is collapsed by the application of an external force. In z-pinch scheme, the conductor is plasma that implodes by the  $J \times B$  force due to a large current flowing through it. The subject of magnetic field compression by imploding plasma has gained particular interest due to the advances in producing plasmas of high temperature and density for fusion purposes, based on the approach of magnetized plasma compression [1].

### 2. EXPERIMENTAL SETUP

In our configuration (see Figure 1a), a cylindrical argon gas-puff shell (initial radius 19 mm and mass per length 30  $\mu\text{g}/\text{cm}$ ), in which a quasi-static axial magnetic flux ( $B_{z0} \leq 0.4$  T) is pre-embedded, pre-fills the anode-cathode gap (10 mm). Subsequently, a pulsed-current (rising to 300 kA in 1.6  $\mu\text{s}$ ) is driven through the gas, ionizes it, and generates an azimuthal magnetic field,  $B_\theta$ , creating a pressure that compresses the plasma radially inward together with the embedded  $B_z$ -field. The initial  $B_{z0}$  is generated by a pair of Helmholtz coils (HC) carrying a long current pulse ( $\sim 5$  ms) to allow for the diffusion of  $B_z$  into the anode-cathode gap.

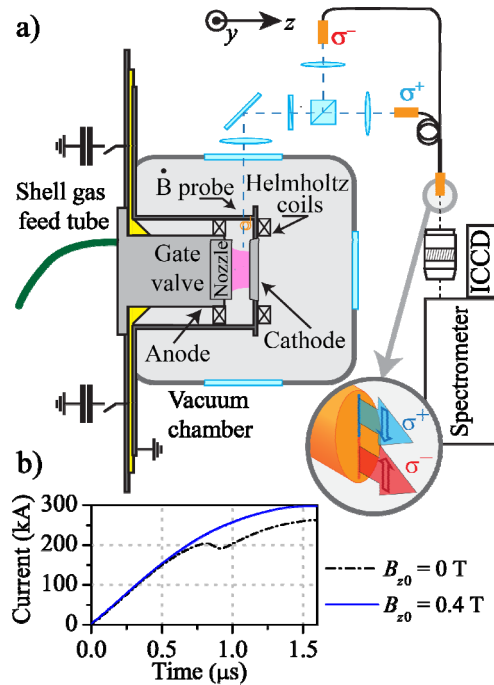


Figure 1. a) Schematic description of the experimental setup and spectroscopic system used for  $B_0$  measurements. b) Current traces for  $B_{z0} = 0$  and  $B_{z0} = 0.4$  T.

Spectroscopic technique for  $B_0$  measurements is recently developed and described in Refs. [2,3]. When the plasma emission is viewed parallel to the B-field,  $\sigma^+$  and  $\sigma^-$  circularly polarized Zeeman components are observed. These two components are separated using polarization optics, consisting of a quarter-wave plate and a polarizing beam splitter. Each of the two components, now linearly polarized, is imaged on a separate linear array of 50 optical fibers. The two ends of the fiber arrays are imaged along the entrance slit of a high-resolution imaging spectrometer, coupled with ICCD. This setup allows for a simultaneous recording of the two polarization components ( $\sigma^+$  and  $\sigma^-$ ), emitted from the same plasma volume in a single discharge, on different parts of a single ICCD detector. Within addition to the spectroscopic measurements, a calibrated B-dot probe is used for measuring the total load current that flows through the discharge.

### 3. RESULTS

$B_0$  is determined using the  $\sigma^+$  and  $\sigma^-$  Zeeman components of the Ar III line ( $^4S$ ) $4s$   $^5S_2$  - ( $^4S$ ) $4p$   $^5P_2$  at  $\lambda = 3301.85$  Å. Figure 2a presents a typical spectral image obtained at  $z = 5$  mm, for  $B_{z0} = 0$  ( $z = 0$  is the anode surface) and at  $t = 806$  ns ( $t = 0$  is the beginning of the current pulse, gate time is 10 ns). The upper and lower halves of the figure show the spatially resolved (in the  $r$ -direction) plasma emission of the  $\sigma^+$  and  $\sigma^-$  components, respectively. The upper branch of the fiber array is flipped, such that the emission from the plasma outer radii

are recorded close to the center of the ICCD, to minimize the effects of optical aberrations. Figure 2b shows the lineouts shapes of the  $\sigma^+$  and  $\sigma^-$  Zeeman components at the outermost plasma radius ( $r_{\text{imp}} = 7.8$  mm, marked by the rectangles in Fig. 2a), along with their best fits.

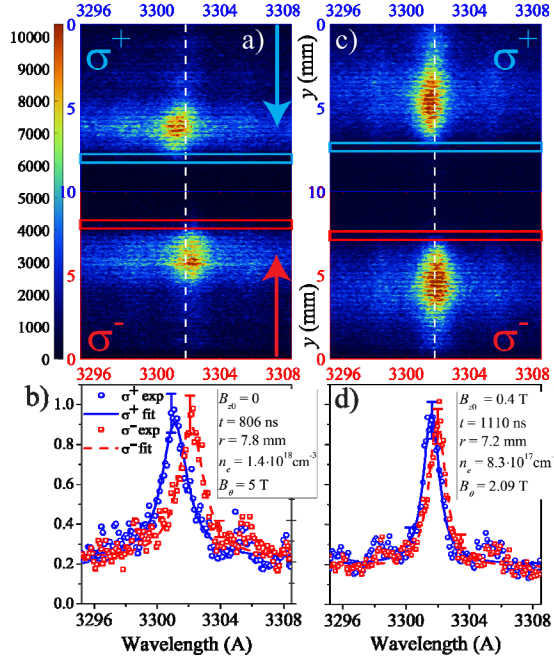


Figure 2. a) Spectral image of the Ar III 4s-4p transition ( $\lambda = 3301.85 \text{ \AA}$ ), for  $B_{z0} = 0$ ; b) spectral line shapes of the  $\sigma^+$  (blue circles) and  $\sigma^-$  (red squares) Zeeman components along with the best fits (blue solid and red dashed lines); c) spectral image for  $B_{z0} = 0.4 \text{ T}$ ; d) explanations are the same as in b). The dashed white vertical line in a) and c) represents un-shifted position of the line center ( $B_{\theta} = 0$ ). The horizontal lines mark the lineout positions.

Each of  $\sigma^+$  and  $\sigma^-$  line shapes are fitted with a Voigt profile, where the Gaussian part accounts for both the instrumental and Doppler broadenings, and the Lorentzian part that is due to the Stark broadening. The influence of the Zeeman effect on the spectral shape of each of the  $\sigma$ -component is small.  $B_{\theta}$  is then extracted from the wavelength difference between the peaks of the best fits. Figures 2c-d are the same as Figures 2a-b, but for  $B_{z0} = 0.4 \text{ T}$ , obtained at  $t = 1100 \text{ ns}$ .

The imploding plasma radii observed from the spectral images in Figures 2a and c are similar. Assuming the entire current is flowing through the imploding plasma, we expect that  $B_{\theta}$  would be lower for the case of  $B_{z0} = 0$ , due to the significantly smaller current measured by the B-dot probe at the time of the spectra recording ( $\sim 195 \text{ kA}$  for  $B_{z0} = 0$  compared to  $\sim 270 \text{ kA}$  for  $B_{z0} = 0.4 \text{ T}$ , as seen from Figure 1b). However, while the measured  $B_{\theta}$  in the case of  $B_{z0} = 0$ , is  $B_{\theta} = 5 \text{ T}$ , as expected, in the case of  $B_{z0} = 0.4 \text{ T}$ , the measured  $B_{\theta} = 2.1 \text{ T}$  is much lower than expected from Ampere's law. Measurements during the implosion phase at different  $z$ -position also confirm the discrepancy between expected and measured values of  $B_{\theta}$  for  $B_{z0} > 0 \text{ T}$ . In contrast, for  $B_{z0} = 0$ , the expected and measured  $B_{\theta}$  values are practically the same. This means that for  $B_{z0} = 0$  the entire current flows within the imploding argon

shell. On the other hand, for  $B_{z0} = 0.4$  T, only  $\sim 1/4$  of the current is flowing through the imploding argon plasma.

Spectroscopic measurements revealed the existence of low-density-plasma (LDP) at  $20 \leq r \leq 27$  mm, for  $B_{z0} = 0.4$  T, that consists of argon and hydrocarbon impurities ( $10^{16} \leq n_{eLDP} \leq 10^{17}$  cm $^{-3}$ ,  $4 \leq T_{eLDP} \leq 6.5$  eV, while the typical plasma parameters of the main imploding argon plasma are  $n_e(\text{Ar}) \sim 10^{18}$  cm $^{-3}$  and  $T_e(\text{Ar}) \sim 5$  eV).  $B_\theta$  measurements at the outer edge of this LDP ( $r \approx 27$  mm), obtained using Zeeman splitting of the C IV,  $\lambda = 5801.33$  Å revealed that the current flowing within  $r \leq 27$  mm accounts for nearly the entire current measured by the B-dot, providing a definite answer for the missing current in the imploding plasma. LDP is also observed when  $B_{z0} = 0$ , but it is of lower density and temperature ( $n_e \leq 3 \cdot 10^{16}$  cm $^{-3}$  and  $T_e \leq 2$  eV), that remain low throughout the implosion, consistent with the absence of a significant current flowing through the LDP. It is only in the presence of  $B_{z0} > 0$  that the LDP carries a significant part of the current. Although, much of the current flows through the LDP at large radii, this LDP is only slowly imploding. The development of a force-free current configuration can be an explanation to this phenomenon.

#### 4. CONCLUSIONS

The significant effects of  $B_{z0}$  on the implosion dynamics are due to current loss to the LDP. Previously unpredicted observations in high-power magnetized-plasma experiments, like (i) formation of helical structures (observed in the Magnetized Liner Inertial Fusion experiment [1]), (ii) larger-than-predicted implosion time and plasma radius at stagnation, and (iii) reduction of the continuum and K-shell emission, may be connected and explained by the present discovery.

#### ACKNOWLEDGEMENTS

This work is supported in part by the Cornell Multi-University Center for High Energy Density Science (USA), Israel Science Foundation and United States-Israel Binational Science Foundation.

#### REFERENCES

- [1] M. R. Gomez, et. al., Phys. Rev. Lett., 113, 155003, (2014)
- [2] G. Rosenzweig, E. Kroupp, A. Fisher, and Y. Maron, JINST 12, P09004 (2017)
- [3] D. Mikitchuk, M. Cvejć, R. Doron, E. Kroupp, C. Stollberg, Y. Maron, A. L. Velikovich, N.D. Ouart, J. L. Giuliani, T.A. Mehlhorn, E.P. Yu and A. Fruchtman, submitted to Phys. Rev. Lett.